Mutation of the MAP kinase DYF-5 affects docking and undocking of kinesin-2 motors and reduces their speed in the cilia of *Caenorhabditis elegans*

Jan Burghoorn*, Martijn P. J. Dekkers*, Suzanne Rademakers*, Ton de Jong†, Rob Willemsen‡, and Gert Jansen*§

*Department of Cell Biology and Genetics and Center for Biomedical Genetics and Departments of †Pathology and ‡Clinical Genetics, Erasmus Medical Center, P.O. Box 2040, 3000 CA, Rotterdam, The Netherlands

Edited by Kathryn V. Anderson, Sloan–Kettering Institute, New York, NY, and approved March 12, 2007 (received for review August 14, 2006)

In the cilia of the nematode *Caenorhabditis elegans*, anterograde intraflagellar transport (IFT) is mediated by two kinesin-2 complexes, kinesin II and OSM-3 kinesin. These complexes function together in the cilia middle segments, whereas OSM-3 alone mediates transport in the distal segments. Not much is known about the mechanisms that compartmentalize the kinesin-2 complexes or how transport by both kinesins is coordinated. Here, we identify DYF-5, a conserved MAP kinase that plays a role in these processes. Fluorescence microscopy and EM revealed that the cilia of *dyf-5* loss-of-function (lf) animals are elongated and are not properly aligned into the amphid channel. Some cilia do enter the amphid channel, but the distal ends of these cilia show accumulation of proteins. Consistent with these observations, we found that six IFT proteins accumulate in the cilia of *dyf-5(lf)* mutants. In addition, using genetic analyses and live imaging to measure the motility of IFT proteins, we show that *dyf-5* is required to restrict kinesin II to the cilia middle segments. Finally, we show that, in *dyf-5(lf)* mutants, OSM-3 moves at a reduced speed and is not attached to IFT particles. We propose that DYF-5 plays a role in the undocking of kinesin II from IFT particles and in the docking of OSM-3 onto IFT particles.

cilia length | *dyf-5* | intraflagellar transport

Cilia are present on almost every vertebrate cell and have important functions in motility or sensation. Within cilia, structural components and signaling molecules are transported by a specialized system, called intraflagellar transport (IFT) (1–5). Transport from the base of the cilia to the tip (anterograde) is mediated by kinesin-2 motor complexes, whereas dynein motor complexes mediate transport back to the base (retrograde). The nematode *Caenorhabditis elegans* has 60 ciliated neurons, including eight pairs of amphid neurons exposed to the environment (6). The cilia of these neurons can be divided into a middle segment with nine doublet microtubules and a distal segment with nine singlet microtubules (7). In the middle segments, two distinct kinesin-2 motor complexes mediate anterograde transport, heterotrimeric kinesin II, encoded by *klp-11*, *klp-20*, and *kap-1* and homodimeric OSM-3 kinesin (8). In the distal segments, transport is mediated by only OSM-3 (8). Live imaging of the movement of these kinesins suggests that kinesin II alone moves at 0.5 μm/s, and OSM-3 alone moves at 1.3 μm/s, whereas the two motor complexes together move at 0.7 μm/s (8). Recently, Pan *et al.* (9) have shown that these *in vivo* transport rates can be reconstituted *in vitro* by using purified kinesin II and OSM-3 motors. Thus far, two proteins have been identified that are required to stabilize IFT complexes transported by both kinesin II and OSM-3, BBS-7 and BBS-8 (10). However, it remains unclear how kinesin II is restricted to the cilia middle segments, whereas OSM-3 is allowed to enter the distal segments and what the functional significance is of this compartmentalization.

Recently, Evans *et al.* (11) have suggested that differences in the activities of the two kinesins contribute to morphological and functional differences between the cilia of individual neurons. Not much is known about the molecular mechanisms that control length and morphology of cilia, although it has been proposed that cilia length is controlled by a balance between cilia assembly and disassembly regulated by IFT (12–14). Genetic approaches have thus far identified three proteins involved in the regulation of cilia length: two *Chlamydomonas reinhardtii* proteins, LF1 and LF2, and the *Chlamydomonas* MAP kinase LF4 and its *Leishmania mexicana* homologue LmxMPK9 (15–18).

The identification of genes involved in IFT in *C. elegans* has profited significantly from the fact that a subset of *C. elegans*' amphid neurons exposed to the environment can take up fluorescent dyes via their cilia, a process called dye-filling (19). This phenomenon has allowed the identification of mutants with cilia defects, often caused by mutations in components of the IFT machinery (1, 2, 7, 20). Here, we describe the identification of the gene mutated in *dyf-5* animals, a dye filling-defective (Dyf) mutant isolated previously in a forward genetic screen (20). *dyf-5* encodes a predicted serine–threonine kinase homologous to three human MAP kinases with unknown functions, *Chlamydomonas* LF4 and *Leishmania* LmxMPK9. We found that mutations in *dyf-5* affect cilia length and morphology. We also show that *dyf-5(lf)* affects the constitution and coordination of IFT particles. First, kinesin II can enter the distal segments in *dyf-5(lf)* mutants. Second, OSM-3 is separated from the IFT particles and moves at a reduced speed in *dyf-5(lf)* mutants. Third, *dyf-5(lf)* animals show accumulation of six different IFT proteins in the cilia.

Results

***dyf-5* Encodes a Conserved MAP Kinase.** *dyf-5* has been mapped to a small region of chromosome I (20). We identified *dyf-5* as M04C9.5 using transgenic rescue and candidate gene sequencing (Fig. 1*A*). Independently, others have also identified the *dyf-5* gene (21).

dyf-5(mn400) contains a G-to-A transition in exon 3 (Fig. 1*A*), which introduces a stop codon at amino acid position 49. In addition, we characterized two deletion alleles of *dyf-5*, *ok1170* and *ok1177*, generated by the *C. elegans* gene knockout consortium. Both deletion alleles remove most of the *dyf-5* coding region and are very likely null alleles (Fig. 1*A*). All three *dyf-5(lf)* alleles show Dyf phenotypes (Fig. 1 *B* and *C* and results not shown). Dye-filling could be restored by introducing low concentrations (5 ng/μl) of a 7.5-kb genomic fragment containing the M04C9.5 gene or a full-length *dyf-5::gfp* fusion construct in *dyf-5(ok1170)* and *dyf-5(mn400)* animals (Fig. 1*D* and results not shown), confirming that this gene

Author contributions: J.B. and M.P.J.D. contributed equally to this work; G.J. designed research; J.B., M.P.J.D., S.R., T.d.J., R.W., and G.J. performed research; J.B., M.P.J.D., and G.J. analyzed data; and J.B., M.P.J.D., and G.J. wrote the paper.

The authors declare no conflict of interest.

This article is a PNAS Direct Submission.

Abbreviations: IFT, intraflagellar transport; lf, loss-of-function.

§To whom correspondence should be addressed at: Department of Cell Biology and Genetics, Erasmus Medical Center, P.O. Box 2040, 3000 CA, Rotterdam, The Netherlands. E-mail: g.jansen@erasmusmc.nl.

This article contains supporting information online at www.pnas.org/cgi/content/full/0606974104/DC1.

GENETICS

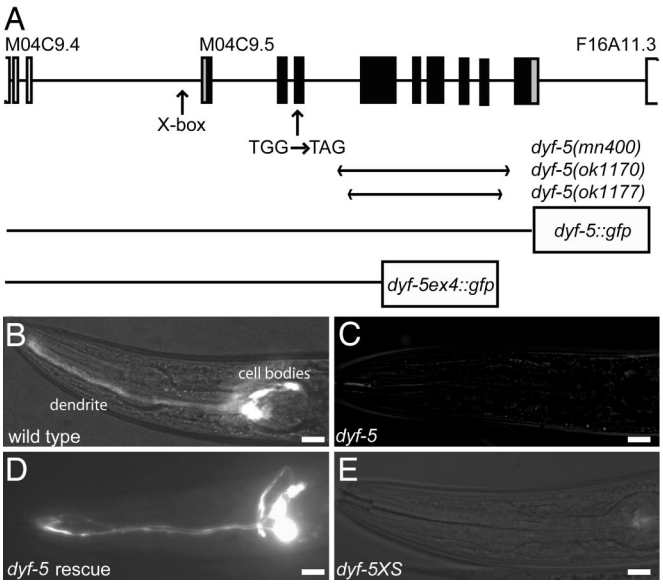

Fig. 1. *dyf-5* encodes a putative protein kinase. (*A*) Schematic representation of the *dyf-5* gene structure (M04C9.5). Coding exons are indicated as black boxes; 5′ and 3′ UTR are depicted as gray boxes. Exons of the flanking genes are indicated as open boxes. The predicted X-box is indicated. Arrows indicate the position of the G-to-A substitution in *dyf-5(mn400)* animals, and the regions deleted in the *ok1170* and *ok1177* alleles. The two *dyf-5*::*gfp* fusion constructs have been indicated. (*B–E*) DiI dye-filling of wild-type (*B*), *dyf-5(mn400)* (*C*), *dyf-5(ok1170) gjEx824(dyf-5)* rescue strain (*D*), and *dyf-5XS(gjEx817)* (*E*) animals. Both *dyf-5(lf)* and *dyf-5(XS)* animals are dye-filling-defective. (Scale bars, 20 μm.) Anterior is to the left.

indeed encodes *dyf-5*. Transgenic animals carrying high copy numbers of the *dyf-5* gene (*dyf-5XS*, injected with 75 ng/μl) or the full-length *dyf-5*::*gfp* construct showed dye-filling defects (Fig. 1*E* and results not shown), suggesting that the levels of DYF-5 are important for its function.

Characterization of the *dyf-5* gene structure using RT-PCR identified an additional upstream exon as well as some errors in the predicted M04C9.5 gene structure. We have communicated the confirmed *dyf-5* gene structure to Wormbase (www.wormbase.org). *dyf-5* encodes a protein of 471 aa, which shows extensive homology to three mammalian proteins that form a small subfamily of MAP kinases. This subfamily consists of MAK (male germ cell-associated kinase) (22), ICK or MRK (intestinal cell kinase and MAK-related kinase, respectively) (23, 24), and MOK (MAPK/MAK/MRK overlapping kinase) (25), with highly conserved N-terminal catalytic domains and more divergent C-terminal noncatalytic domains. Although the functions of these kinases in mammals are not known, studies in other organisms suggest a function in the cilia. Mutations in a DYF-5 homologue in *Leishmania mexicana*, LmxMPK9 (17), and in one of the two homologues in *Chlamydomonas reinhardtii*, LF4 (18), affect the length of the flagella of these organisms. In addition, several genome-wide approaches have identified DYF-5 and its homologues as likely ciliary proteins (21, 26–30).

***dyf-5* Functions in Ciliated Neurons.** We examined the expression pattern of *dyf-5* using two *dyf-5*::*gfp* fusion constructs: a full-length, functional *dyf-5*::*gfp* fusion and a construct in which GFP is fused in frame to the fourth exon of *dyf-5* (*dyf-5ex4*::*gfp*) (Fig. 1*A*). The full-length *dyf-5*::*gfp* construct showed weak GFP expression in many neurons in the head, including amphid and labial sensory neurons (Fig. 2*A*) and three pairs of neurons in the tail, including the phasmid sensory neurons. In addition, we observed expression in many cells in the male tail (Fig. 2*B*). This DYF-5::GFP fusion

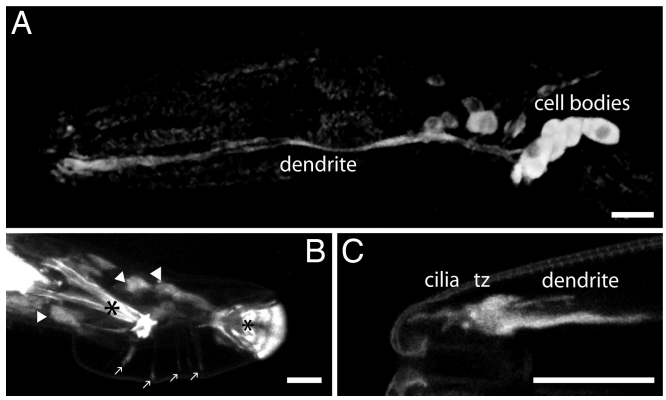

Fig. 2. *dyf-5*::*gfp* expression pattern. (*A*) Expression of *dyf-5*::*gfp* in the dendrites and cell bodies of many neurons, including amphid sensory neurons in the head. (*B*) Strong *dyf-5*::*gfp* expression in many neurons in the male tail. Cell bodies are indicated with arrowheads, expression in the sensory rays is indicated with arrows, and autofluorescence of the spicule and the posterior end of the fan is indicated with asterisks. (*C*) Strong *dyf-5*::*gfp* expression in the tip of the head in dendrites and transition zone (tz) and weakly in cilia. [Scale bars, 20 μm (*A* and *B*) or 10 μm (*C*).] Anterior is to the left.

could be detected uniformly in axons, cell bodies, and dendrites. In addition, we observed strong fluorescence at the transition zones, which connect the cilia with the dendrites, and weak fluorescence uniformly in the cilia (Fig. 2*C*). The *dyf-5ex4*::*gfp* fusion construct essentially showed the same *dyf-5* expression pattern, albeit stronger and more restricted to the cell bodies. In addition, DYF-5ex4::GFP could be detected in the CAN cells, neurons associated with the excretory canal (6) and in a pair of neurons in the posterior lateral ganglion (results not shown).

Expression of many ciliary genes is regulated by the DAF-19 transcription factor (31). This regulation occurs through an X-box promoter element. The *dyf-5* promoter region contains a predicted X-box promoter element, 193 bp upstream of the SL1 trans splice site and 271 bp upstream of the translational start (Fig. 1*A*). Previous genomic analyses have identified many genes that contain X-box elements, including M04C9.5 (21, 26, 28). Chen *et al.* (21) have confirmed that expression of *dyf-5* is indeed regulated by *daf-19*.

Mutation of *dyf-5* Affects Cilia Morphology and Length. We wondered whether mutations in *dyf-5* affect cilia morphology and length, as in *Chlamydomonas* and *Leishmania* (17, 18). Visualization of the microtubular axonemes of the cilia using anti-tubulin antibodies revealed that the cilia of *dyf-5(lf)* animals were not properly aligned into the amphid pore. The cilia were more dispersed, misdirected, and sometimes turned back toward the transition zone (Fig. 3*B*). In contrast, in the two *dyf-5XS* strains, *gjIs828* and *gjIs831*, we observed very weak anti-tubulin staining and only very short or no cilia structures (results not shown).

To study the morphological defects in more detail, we examined cross-sections of wild-type and *dyf-5(lf)* animals with EM. In the wild-type animal, the 10 cilia were enveloped by the sheath cell and projected to the tip of the animal, where the cilia ended in a channel lined by the socket cell (Fig. 3 *C* and *D*; refs. 7, 32, and 33). The microtubular axoneme in the middle segment consisted of a ring of nine doublet microtubules and up to six singlet microtubules (Fig. 3*D*) (7, 32, 33). In the tip of the cilium the nine microtubules were all singlets (Fig. 3*D*) (7, 32, 33). In the *dyf-5(lf)* mutant, the morphology of the cilia was severely affected. In the most proximal section, the cilia were more dispersed, consistent with the anti-tubulin data (Fig. 3*D*). We could not identify all 10 cilia, perhaps because of their dispersion and their altered morphology. In the cilia, the microtubular axoneme consisted of an array of singlet and

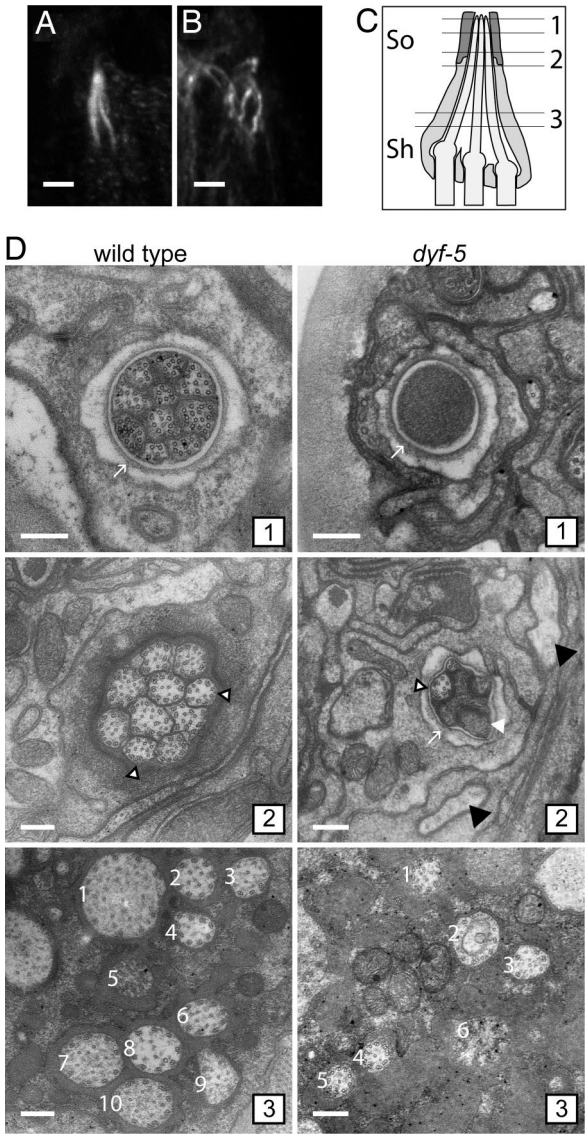

Fig. 3. Mutation of *dyf-5* affects cilia length and morphology. (*A* and *B*) Anti-tubulin immunostaining of wild-type (*A*) and *dyf-5(ok1177)* (*B*) animals. (Scale bar, 2 μm.) Anterior is up. (*C*) Schematic representation of three of the amphid channel cilia embedded in the sheath cell (sh) and the socket cell (so). The approximate positions of the EM cross-sections in *D* have been indicated. (*D*) EM cross-section of a wild-type (*Left* 1–3) and *dyf-5(lf)* (*Right* 1–3) animal (1). Sections through the socket cell (arrow), showing the distal segments of the 10 channel cilia that contain singlet microtubules in the wild-type animal and the channel filled with electron-dense material in the *dyf-5(lf)* animal (2). Ten channel cilia embedded in the sheath cell are present in the wild-type animal. Most cilia contain doublet microtubules; some contain singlets (open arrowheads). Section of a *dyf-5(lf)* animal through the socket cell (arrow), showing some cilia with singlet microtubules (open arrowhead) and some cilia filled with electron-dense material (white arrowhead). Black arrowheads indicate oblique sections through cilia (3). Sections through the middle segments close to the base of the cilia. In the wild-type animal, 10 channel cilia (numbered 1–10) embedded in the sheath cell are present, containing doublet microtubules. In the *dyf-5(lf)* animal, six channel cilia (1–6) embedded in the sheath cell could be identified, containing doublet microtubules. The cilia are more dispersed than in wild-type animals. (Scale bars, 200 nm.)

doublet microtubules (Fig. 3*D*). More distally, we observed some cilia entering into the channel, indicating that the socket cell is present and open. At this level, the microtubules were singlets. Not all cilia entered the channel. Next to the socket cell, we observed two structures resembling oblique sections through cilia, which could be misdirected channel cilia (Fig. 3*D*). In the most distal sections, the channel was completely filled with electron-dense matrix material, probably accumulated proteins (Fig. 3*D*).

To study the effect of *dyf-5(lf)* on the morphology of individual amphid cilia, we examined transgenic animals expressing *gpa-4*::*gfp* or *gpa-15*::*gfp*. The Gα subunits *gpa-4* and *gpa-15* are expressed in only the ASI amphid neurons or in the ADL, ASH, and ASK neurons, respectively (34) and localized along the length of the cilia in wild-type animals (Fig. 4 *A* and *J*). Again, we observed that the cilia were more dispersed and misdirected. In addition, the cilia of *dyf-5(lf)* animals were significantly longer than cilia of wild-type animals (Fig. 4 *B* and *K* and Table 1). In contrast, in *dyf-5XS* animals, we observed very short cilia or, in 27% of the animals, no discernible cilia at all (Fig. 4 *C* and *L* and Table 1).

The above-described approaches all showed similar effects of *dyf-5(lf)* on the length and morphology of the cilia. To determine whether *dyf-5* regulates cilia length in a cell-autonomous fashion, we expressed the full-length *dyf-5*::*gfp* construct specifically in the ASI neurons of *dyf-5(lf)* animals and determined the lengths of the ASI cilia of these animals by using *gpa-4*::*gfp*. In two of the five transgenic lines that expressed *dyf-5*::*gfp* specifically in the ASI neurons, the cilia were significantly shortened, to approximately wild-type length (Table 1). These results indicate that *dyf-5* functions cell-autonomously to regulate cilia length.

Kinesin II Localizes to the Distal Segments in *dyf-5(lf)* Animals. Next, we wondered whether elongation of the cilia in *dyf-5(lf)* animals requires the function of either of the two anterograde motors, kinesin II or OSM-3. To this end, we generated *dyf-5(lf); kap-1* and *dyf-5(lf); osm-3* double mutants. *osm-3* animals lack the cilia distal segments, because OSM-3 is essential for transport in these segments (8) (Fig. 4 *F* and *O*). *kap-1* animals have lost an essential component of the heterotrimeric kinesin II complex but have full-length cilia, because OSM-3 can mediate IFT by itself (8) (Fig. 4 *D* and *M*).

Both *dyf-5(lf); osm-3* and *dyf-5(lf); kap-1* double-mutant animals were dye filling-defective (results not shown). Anti-tubulin antibody staining and *gpa-4*::*gfp* and *gpa-15*::*gfp* fluorescence showed that the cilia of both double mutants were as long as or even longer than the *dyf-5(lf)* cilia (Fig. 4 *E*, *G*, *N*, and *P* and Table 1). This suggests that both motors can transport cargo along the full length of the cilia and, thus, that DYF-5 is required to restrict kinesin II to the middle segments. In addition, these results suggest that the elongation of the cilia in *dyf-5(lf)* does not depend solely on either of the two kinesin-2 motors.

Interestingly, we observed an additional morphological defect of the cilia of *dyf-5(lf); kap-1* animals: in 30% of the animals, the cilia were branched (Fig. 4*E*), a defect that was observed in only 7% of *dyf-5(lf)* animals and never in wild-type or *kap-1* animals. In *dyf-5(lf); osm-3* animals, branching was observed in only 1 animal of 33 analyzed. These results suggest that DYF-5 and kinesin II both play a role in cilium morphogenesis.

To determine whether transport in the cilia of *dyf-5(lf)* animals can be mediated by a kinesin II- and OSM-3-independent mechanism, we generated *dyf-5(lf); kap-1; osm-3* triple-mutant animals. Visualization of the cilia using anti-tubulin antibodies and *gpa-4*::*gfp* and *gpa-15*::*gfp* showed that these triple mutants have no or only very short cilia, similar to *kap-1; osm-3* animals (Fig. 4 *H*, *I*, *Q*, and *R* and Table 1), indicating that either kinesin II or OSM-3 is required for ciliogenesis.

Because both kinesin-2 motors are individually dispensable for cilia elongation in *dyf-5(lf)* animals, we analyzed the localization of OSM-3::GFP and KAP-1::GFP fusion constructs in *dyf-5(lf)* animals (8). In wild-type animals, OSM-3::GFP could be detected along the length of the cilia, whereas KAP-1::GFP could be detected only in the cilia middle segment (Fig. 5 *A*–*C*), as reported (8). In *dyf-5(lf)* animals, OSM-3::GFP could be detected along the full length of the cilia. Additionally, we observed strong accumu-

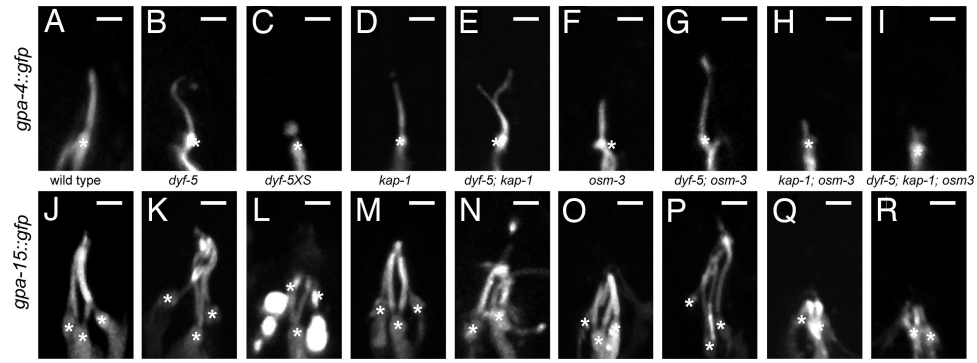

Fig. 4. Mutation of *dyf-5* affects cilia length. Visualization of ASI cilia structures using *gpa-4*::*gfp* (*A–I*) and ADL, ASH, and ASK cilia morphology using *gpa-15*::*gfp* (*J–R*) in wild-type (*A* and *J*), *dyf-5(ok1177)* (*B* and *K*), *dyf-5XS(gjIs828)* (*C* and *L*), *kap-1(ok676)* (*D* and *M*), *dyf-5; kap-1* (*E* and *N*), *osm-3(p802)* (*F* and *O*), *dyf-5; osm-3* (*G* and *P*), *kap-1; osm-3* (*H* and *Q*), and *dyf-5; kap-1; osm-3* (*I* and *R*) animals. In *dyf-5*, *dyf-5; kap-1*, and *dyf-5; osm-3* animals, cilia were elongated and misdirected. In *dyf-5XS* animals, cilia were very short or could not be detected. We observed branching of the cilia in 30% of *dyf-5; kap-1* animals. Transition zones are indicated with asterisks. (Scale bars, 2 μm.) Anterior is up.

lation of OSM-3::GFP starting ≈2–3 μm from the transition zone and in the distal region of the cilia (Fig. 5*H*). Also KAP-1::GFP fluorescence could be seen along the full length of the cilia of *dyf-5(lf)* animals (Fig. 5*G*), confirming that DYF-5 is required to restrict KAP-1::GFP to the middle segments. We also observed accumulation of KAP-1::GFP halfway along the cilia. *dyf-5XS* animals showed both OSM-3::GFP and KAP-1::GFP fluorescence at the transition zones, but not at all or only very weakly in the cilia of these animals (results not shown), confirming that *dyf-5* overexpression blocks cilia assembly.

To determine whether the localization of other IFT proteins was affected, we used a *che-11*::*gfp* fusion construct to visualize this complex-A IFT protein (35), a *che-13*::*gfp* fusion construct and anti-OSM-5 antibodies to visualize these two complex-B proteins (35–37), and *xbx-1*::*gfp* to visualize the dynein complex (38). All these IFT proteins could be detected along the length of the cilia of *dyf-5(lf)* animals, and they all showed accumulation starting approximately halfway along the cilia and into the distal segments (Fig. 5 *D–F* and *I–K* and results not shown). Also *dyf-5(lf); kap-1* and *dyf-5(lf); osm-3* double-mutant animals showed accumulation of CHE-11 and OSM-5 in the cilia (results not shown), suggesting that these effects of *dyf-5(lf)* do not depend on either kinesin II or OSM-3.

Table 1. Cilia lengths of *dyf-5* mutant animals

	gpa-4::*gfp*		*gpa-15*::*gfp*	
Genotype	Length, μm	*n*	Length, μm	*n*
Wild type	4.94 ± 0.57	60	6.83 ± 0.40	40
dyf-5	5.66 ± 0.97*	83	8.62 ± 0.86*	30
dyf-5XS(gjIs828)	1.89 ± 0.49*	18	ND	
dyf-5XS(gjIs831)	2.13 ± 0.66*	15	4.56 ± 0.72*	28
kap-1	4.78 ± 0.24	23	6.79 ± 0.40	31
dyf-5; kap-1	5.48 ± 1.11†‡	54	8.32 ± 1.23*‡	50
osm-3	3.77 ± 0.32*	24	4.89 ± 0.47*	41
dyf-5; osm-3	6.48 ± 0.86*§¶	43	8.70 ± 1.35*¶	47
kap-1; osm-3	1.84 ± 0.31*‡¶	26	ND	
dyf-5; kap-1; osm-3	1.86 ± 0.39*‡§¶	23		ND
dyf-5; gjEx312	4.96 ± 0.97‖	24	ND	
dyf-5; gjEx324	4.83 ± 0.83§	22	ND	

Indicated are the average lengths of GPA-4::GFP and GPA-15::GFP staining cilia ±SD, the significance tested by using a two-tailed paired *t* test compared with wild-type animals (*, $P < 0.001$; †, $P < 0.005$); *kap-1* (‡, $P < 0.001$); *dyf-5* (§, $P < 0.001$; ‖, $P < 0.005$); and *osm-3* (¶, $P < 0.001$), and the number of animals (*n*). The *dyf-5XS* cilia lengths indicated represent the lengths of the cilia where cilia could be seen; in an additional 27%, no cilia could be detected. *gjEx312* and *gjEx324* are two independent *gpa-4*::*dyf-5*::*gfp* strains that express *dyf-5* only in the ASI neurons. ND, not determined.

***dyf-5(lf)* Separates the OSM-3 Motor from IFT Particles.** Because DYF-5 is required to restrict kinesin II to the cilia middle segments, we wondered whether *dyf-5(lf)* affects the transport rates of the two kinesin-2 motors. In the middle segments of wild-type animals,

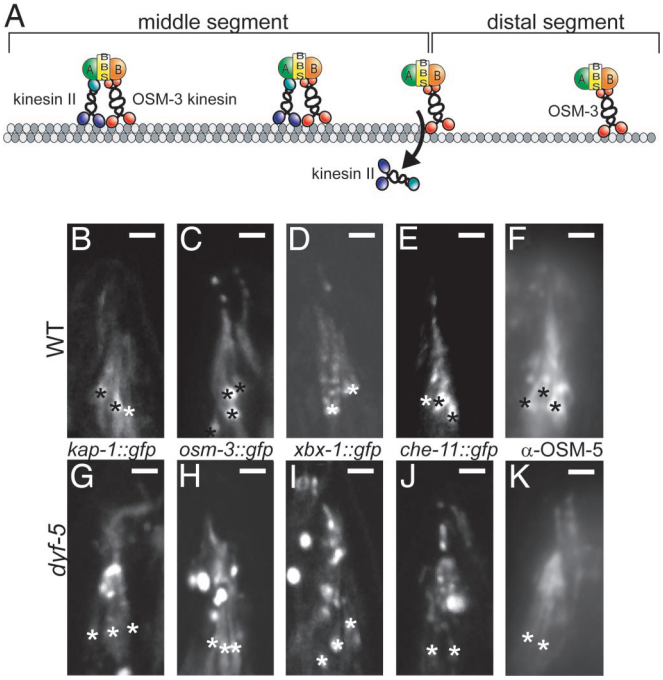

Fig. 5. DYF-5 is required to restrict kinesin II to cilia middle segments. (*A*) Model of anterograde IFT in *C. elegans* (based on model in ref. 10). In the cilia middle segments, cargo is transported by IFT particles that contain OSM-3 kinesin-2, kinesin II, complex A (*A*) and B (*B*) proteins and the BBS-7 and BBS-8 proteins (BBS). At the end of the middle segments, kinesin II is probably released from the IFT particle. Transport in the distal segment is mediated by OSM-3. (*B–K*) Visualization of KAP-1::GFP (*B* and *G*), OSM-3::GFP (*C* and *H*), XBX-1::GFP (*D* and *I*), CHE-11::GFP (*E* and *J*), and OSM-5 (*F* and *K*) in wild-type (*B–F*) and *dyf-5(ok1170)* (*G–K*) animals. All IFT proteins, including KAP-1::GFP, could be detected along the length of the cilia of *dyf-5* animals. We observed accumulation of all IFT proteins, approximately halfway along the cilia and in the distal segment. Because these GFP constructs are expressed in all channel cilia, it was impossible to determine the length of a specific cilium. Transition zones are indicated with asterisks. (Scale bars, 2 μm.) Anterior is up.

Table 2. *dyf-5* separates the OSM-3 motor from IFT particles

		Middle segment		Distal segment	
IFT particle	Genotype	Speed, μm/s	*n*	Speed, μm/s	*n*
KAP-1::GFP	Wild type	0.70 ± 0.14	189		
	osm-3	0.49 ± 0.10*	91		
	dyf-5	0.50 ± 0.12*	110	0.51 ± 0.16	56
OSM-3::GFP	Wild type	0.70 ± 0.19	117	1.14 ± 0.23	43
	kap-1	1.17 ± 0.24*	124	1.23 ± 0.28	42
	dyf-5	0.59 ± 0.15*†	210	0.59 ± 0.17*‡	84
	dyf-5; kap-1	0.58 ± 0.15*	91		
CHE-11::GFP	Wild type	0.69 ± 0.20	118	1.20 ± 0.27	49
	osm-3	0.50 ± 0.09*	90		
	dyf-5	0.49 ± 0.11*	170	0.49 ± 0.11*	45
	dyf-5; kap-1	0.60 ± 0.16*§	118	0.61 ± 0.12*§	38
	dyf-5; osm-3	0.49 ± 0.12*	109	0.49 ± 0.11*	31
OSM-5::GFP	Wild type	0.70 ± 0.17	136	1.13 ± 0.29	66
	osm-3	0.50 ± 0.11*	88		
	dyf-5	0.51 ± 0.11*	151	0.50 ± 0.11*	42
	dyf-5; kap-1	0.59 ± 0.19*§	117	0.58 ± 0.12*§	45
	dyf-5; osm-3	0.51 ± 0.13*	103		
XBX-1::GFP	Wild type	0.70 ± 0.17	141	1.11 ± 0.19	55
	dyf-5	0.50 ± 0.11*	139	0.47 ± 0.08*	42

Indicated are average speeds ±SD and the number of tracks (*n*). Footnotes indicate significant differences when comparing speeds of: *, IFT protein in a mutant background with the same IFT protein in wild type ($P < 0.001$); † and ‡, OSM-3::GFP with the other IFT proteins in *dyf-5(lf)* animals (‡, $P < 0.001$; ‡, $P < 0.01$); and §, CHE-11 and OSM-5 in *dyf-5; kap-1* with their speeds in *dyf-5* and *dyf-5; osm-3* animals. The speeds of all IFT proteins in *dyf-5* and *dyf-5; osm-3* animals, except OSM-3::GFP, were not significantly different from the speeds in *osm-3* animals. Speeds in *dyf-5; kap-1* animals were not significantly different from the speed of OSM-3::GFP in *dyf-5* animals.

kinesin II and OSM-3 traveled jointly at 0.7 μm/s (Table 2). In the absence of kinesin II OSM-3 moved faster (1.15 μm/s), and in the absence of OSM-3, kinesin II moved slower (0.5 μm/s; Table 2). In the distal segments, only OSM-3 is found, moving at a rate of 1.14 μm/s. These speeds are in agreement with previous reports (8). Examples of live imaging of CHE-11::GFP in wild-type and *dyf-5(lf)* animals and corresponding kymographs are given in supporting information (SI) Figs. 6 and 7 and Movies 1 and 2.

We found that, in the middle segments of *dyf-5(lf)* animals, kinesin II traveled at a rate of 0.5 μm/s, and OSM-3 traveled at 0.59 μm/s (Table 2). We found very similar speeds in the distal segments, although imaging was very difficult in these segments because of the twisted appearance of the cilia, often only partly in focus, and accumulation of the GFP fusion proteins. These results suggest that kinesin II and OSM-3 move at least partly separately in the cilia. Ou *et al.* (10) have recently described two mutants that cause separation of kinesin II and OSM-3-mediated transport: *osm-12/bbs-7* and *bbs-8*. In these animals, kinesin II transports the complex-A proteins, and OSM-3 transports the complex-B proteins. To test whether a similar separation occurs in *dyf-5(lf)* animals, we determined the anterograde speeds of the complex-A protein CHE-11, the complex-B protein OSM-5, and the dynein subunit XBX-1. Interestingly, all these proteins moved at 0.5 μm/s in the middle and distal segments of the cilia of *dyf-5(lf)* animals (Table 2), a rate very similar to kinesin II.

The difference in transport rates of kinesin II, CHE-11, OSM-5, and XBX-1 on the one hand and OSM-3 on the other hand suggests that OSM-3 is no longer part of the joint IFT complex in *dyf-5(lf)* animals. However, the speed of OSM-3::GFP observed in *dyf-5(lf)* animals is lower than that of free traveling OSM-3 (Table 1) (8, 10). This effect can be explained by a reduction of the motility of OSM-3 itself. Alternatively, OSM-3 containing particles may be transported predominantly by the slower moving kinesin II, thereby reducing their average speed. To test the latter possibility, we measured transport rates of OSM-3::GFP, CHE-11::GFP, and OSM-5::GFP in *dyf-5(lf); kap-1* and *dyf-5(lf); osm-3* double-mutant animals. We found that, in *dyf-5(lf); kap-1* animals, OSM-3, CHE-11, and OSM-5 moved at 0.59–0.60 μm/s (Table 2), whereas, in *dyf-5(lf); osm-3* animals, CHE-11 and OSM-5 moved at 0.5 μm/s. These findings suggest that the speeds of OSM-3 and kinesin II in *dyf-5(lf)* animals are independent of each other and that these motors indeed move separately. Therefore, we favor the hypothesis that *dyf-5(lf)* reduces the speed of OSM-3 itself. In addition, these results confirm that, in the absence of kinesin II, IFT still can be mediated by OSM-3.

Discussion

In this article, we identify the gene mutated in *dyf-5* animals. DYF-5 encodes a putative MAP kinase that regulates the length of sensory cilia in *C. elegans*, similar to what has been reported for DYF-5 homologues in *Chlamydomonas* (LF4) and *Leishmania* (LmxMPK9) (17, 18): *dyf-5* loss-of-function results in cilia elongation, whereas overexpression results in shorter cilia. In addition, fluorescence and EM showed that, in the absence of DYF-5, the cilia are more dispersed and that many cilia are not properly aligned into the amphid channel and sometimes turn back to the base, although some cilia do enter the channel.

Within the cilia, we find three defects. First, six components of the IFT machinery are not properly localized in *dyf-5(lf)* animals. Interestingly, heterotrimeric kinesin II localizes to the distal segments of *dyf-5(lf)* animals. This is an intriguing finding, because this motor cannot enter this segment of the cilia in wild-type animals. In addition, all six IFT proteins tested accumulate approximately halfway and in the distal regions of the cilia, which correlates with the accumulation of protein seen in these regions by using EM. Second, in *dyf-5(lf)* animals, OSM-3-containing particles travel at a different speed than particles containing either kinesin II, complex-A and -B proteins, or dynein, suggesting that OSM-3 travels separately. In addition, this suggests that DYF-5 functions in a different process than the BBS-7 and BBS-8 proteins, mutations of

which result in separation of complex-A and -B particles (10). Interestingly, OSM-3 can still mediate IFT in *dyf-5(lf)* animals but only in the absence of functional kinesin II. This suggests that inactivation of *dyf-5* does not fully block docking of OSM-3 onto IFT particles, but rather changes the affinity between either of the two kinesins and the IFT particles. Third, the speed of OSM-3 in *dyf-5(lf)* animals was markedly reduced, from 1.2 μm/s to 0.6 μm/s. Our results suggest that this reduced speed is not a result of a combined speed of kinesin II and OSM-3, but rather an effect on OSM-3 itself.

But how does mutation of *dyf-5* mediate these three effects on IFT, and how do these effects correlate with cilia morphology and length? A possible explanation for the effects on the localization of IFT proteins is that DYF-5 functions at sites where the IFT particles switch between different motor complexes, such as the transition from the middle to the distal segment and at the distal tip. Failure in removing kinesin II from IFT particles would explain its entry into the distal segments in *dyf-5(lf)* animals. In addition, a failure in switching from anterograde to retrograde transport would explain the aggregation of IFT proteins in the distal segments. However, such a model does not provide an explanation for the effects that *dyf-5(lf)* has on the speed of OSM-3. The motility of kinesins can be modulated at several levels. For example, the processivity of these motors, and hence their speed, may be reduced by interference with the properties of the kinesin itself, such as ATP binding and hydrolysis or allosteric inhibition of directional movement (39, 40). Also, posttranslational modifications of the microtubules on which the kinesins walk have been reported to affect the motility of kinesins (41). Perhaps DYF-5 functions in a similar manner, changing the affinity of both kinesins for its normal targets, either the IFT particles or the microtubules, resulting in the effects we observe. Interestingly, the entry of kinesin II in the distal segments or the presence of unattached OSM-3 by themselves do not cause the elongation of the cilia of *dyf-5(lf)* animals, because removal of kinesin II or OSM-3 in *dyf-5(lf); kap-1* or *dyf-5(lf); osm-3* animals did not suppress cilia elongation. It will be very interesting to further unravel the mechanisms by which DYF-5 regulates IFT, cilia morphology, and length.

The DYF-5 kinase is conserved in evolution. Using BLAST searches, we have identified putative DYF-5 homologues in various organisms that have cilia: in mammals, *Drosophila*, *Chlamydomonas*, *Leishmania*, and *Trypanosoma* (results not shown). Interestingly, we could not find an obvious homologue in *Plasmodium*, which has cilia, but the cilia are assembled in the cytoplasm in a process that does not require IFT (42). Mammals have three putative DYF-5 homologues that form a small subfamily of MAP kinases, the MAK kinases (22–25). The functions of these MAK, MOK, and ICK/MRK proteins remain to be determined. However, given the evolutionary conservation of the IFT machinery, the DYF-5/MAK kinases and their functions in *C. elegans*, *Chlamydomonas*, and *Leishmania*, we expect that one or more of the mammalian MAK kinases play a role similar to that of DYF-5 in the control of cilia length and the docking and undocking of kinesin-2 motors from IFT particles.

Materials and Methods

Strains and Constructs. All strains were grown at 20°C. Strains and alleles used: Bristol N2 (wild type), *dyf-5(mn400)*I, *dyf-5(ok1170)I*, *dyf-5(ok1177)I*, *kap-1(ok676)III*, *osm-3(p802)IV*, *dyf-5XS(gjIs828)*, and *dyf-5XS(gjIs831)*. *dyf-5::gfp* reporter constructs were generated by using a fusion PCR protocol (43).

Microscopy dye-filling was performed by using DiI (Molecular Probes, Eugene, OR) (19). Immunofluorescence using monoclonal rat antibody against tubulin (ab6160; Abcam, Cambridge, U.K.) and monoclonal mouse antibody against OSM-5 (a kind gift from B. Yoder and C. Haycraft) was performed as described (44).

EM. Animals were fixed in 3% glutaraldehyde for 16 h, followed by postfixation in 1% osmiumtetroxide for 2 h. Epon-embedded animals were cut and stained with uranyl acetate and lead nitrate.

Live Imaging of IFT Particles. Live imaging of the GFP-tagged IFT particles was carried out as described (8). Kymographs were generated in ImageJ with the Kymograph plugin, written by J. Rietdorf. For additional information, see *SI Materials and Methods*.

We thank E. Severijnen, T. de Vries Lentsch, and R. Koppenol for technical assistance; M. Barr (University of Wisconsin, Madison, WI), A. Fire (Stanford University, Stanford, CA), C. Haycraft, and B. Yoder (University of Alabama at Birmingham, Birmingham, AL) G. Ou and J. Scholey (University of California, Davis, CA), the *Caenorhabditis* Genetics Center, and the *C. elegans* Gene Knockout Consortium for *C. elegans* strains and constructs; M. Leroux for discussions; and the members of the G.J. laboratory for critical reading of the manuscript. This work was supported by the Center for Biomedical Genetics and the PKD Foundation. G.J. is a Royal Netherlands Academy of Sciences fellow.

1. Rosenbaum JL, Witman GB (2002) *Nat Rev Mol Cell Biol* 3:813–825.
2. Scholey JM (2003) *Annu Rev Cell Dev Biol* 19:423–443.
3. Qin H, Diener DR, Geimer S, Cole DG, Rosenbaum JL (2004) *J Cell Biol* 164:255–266.
4. Qin H, Burnette DT, Bae YK, Forscher P, Barr MM, Rosenbaum JL (2005) *Curr Biol* 15:1695–1699.
5. Ou G, Qin H, Rosenbaum JL, Scholey JM (2005) *Curr Biol* 15:R410–411.
6. White JG, Southgate E, Thomson JN, Brenner S (1986) *Philos Trans R Soc London Ser B* 314:1–340.
7. Perkins LA, Hedgecock EM, Thomson JN, Culotti JG (1986) *Dev Biol* 117:456–487.
8. Snow JJ, Ou G, Gunnarson AL, Walker MR, Zhou HM, Brust-Mascher I, Scholey JM (2004) *Nat Cell Biol* 6:1109–1113.
9. Pan X, Ou G, Civelekoglu-Scholey G, Blacque OE, Endres NF, Tao L, Mogilner A, Leroux MR, Vale RD, Scholey JM (2006) *J Cell Biol* 174:1035–1045.
10. Ou G, Blacque OE, Snow JJ, Leroux MR, Scholey JM (2005) *Nature* 436:583–587.
11. Evans JE, Snow JJ, Gunnarson AL, Ou G, Stahlberg H, McDonald KL, Scholey JM (2006) *J Cell Biol* 172:663–669.
12. Marshall WF, Rosenbaum JL (2001) *J Cell Biol* 155:405–414.
13. Dentler W (2006) *J Cell Biol* 170:649–659.
14. Pan J, Snell WJ (2005) *Dev Cell* 9:431–438.
15. Tan LW, Dentler WL, Lefebvre PA (2003) *J Cell Biol* 163:597–607.
16. Nguyen RL, Tam LW, Lefebvre PA (2005) *Genetics* 169:1415–1424.
17. Bengs F, Scholz A, Kuhn D, Wiese M (2005) *Mol Microbiol* 55:1606–1615.
18. Berman SA, Wilson NF, Haas NA, Lefebvre PA (2003) *Curr Biol* 13:1145–1149.
19. Hedgecock EM, Culotti JG, Thomson JN, Perkins LA (1985) *Dev Biol* 111:158–170.
20. Starich TA, Herman RK, Kari CK, Yeh WH, Schackwitz WS, Schuyler MW, Collet J, Thomas JH, Riddle DL (1995) *Genetics* 139:171–188.
21. Chen N, Mah A, Blacque OE, Chu J, Phgora K, Bakhoum MW, Newbury CRH, Khattra J, Chan S, Go A, *et al.* (2006) *Genome Biol* 7:R126.
22. Matsushime H, Jinno A, Takagi N, Shibuya M (1990) *Mol Cell Biol* 10:2261–2268.
23. Togawa K, Yan YX, Inomoto T, Slaugenhaupt S, Rustgi AK (2000) *J Cell Physiol* 183:129–139.
24. Yang T, Jiang Y, Chen J (2002) *Biomol Eng* 19:1–4.
25. Miyata Y, Akashi M, Nishida E (1999) *Genes Cells* 4:299–309.
26. Blacque OE, Perens EA, Boroevich KA, Inglis PN, Li C, Warner A, Khattra J, Holt RA, Ou G, Mah AK, *et al.* (2005) *Curr Biol* 15:935–941.
27. Colosimo M, Brown A, Mukhopadhyay S, Gabel C, Lanjuin A, Samuel A, Sengupta P (2004) *Curr Biol* 14:2245–2251.
28. Efimenko E, Bubb K, Mak HY, Holzman T, Leroux MR, Ruvkun G, Thomas JH, Swoboda P (2005) *Development (Cambridge, UK)* 132:1923–1934.
29. Pazour GJ, Agrin N, Leszyk J, Witman GB (2005) *J Cell Biol* 170:103–113.
30. Stolc V, Samanta MP, Tongprasit W, Marshall WF (2005) *Proc Natl Acad Sci USA* 102:3703–3707.
31. Swoboda P, Adler HT, Thomas JH (2000) *Mol Cell* 5:411–421.
32. Ward S, Thomson N, White JG, Brenner S (1975) *J Comp Neurol* 160:313–337.
33. Ware RW, Clark D, Crossland K, Russell RL (1975) *J Comp Neurol* 162:71–110.
34. Jansen G, Thijssen KL, Werner P, van der Horst M, Hazendonk E, Plasterk RH (1999) *Nat Genet* 21:414–419.
35. Qin H, Rosenbaum JL, Barr MM (2001) *Curr Biol* 11:457–461.
36. Haycraft CJ, Swoboda P, Taulman PD, Thomas JH, Yoder BK (2001) *Development (Cambridge, UK)* 128:1493–1505.
37. Haycraft CJ, Schafer JC, Zhang Q, Taulman PD, Yoder BK (2003) *Exp Cell Res* 284:251–263.
38. Schafer JC, Haycraft CJ, Thomas JH, Yoder BK, Swoboda P (2003) *Mol Biol Cell* 14:2057–2070.
39. Carter NJ, Cross RA (2005) *Nature* 435:308–312.
40. Kwok BH, Kaptein LC, Kim JH, Peterman EJG, Schmidt CF, Kapoor TM (2006) *Nat Chem Biol* 9:480–485.
41. Reed NA, Cai D, Blasius TL, Jih GT, Meyhofer E, Gaertig J, Verhey KJ (2006) *Curr Biol* 16:2166–2172.
42. Witman GB (2003) *Curr Biol* 13:R796–R798.
43. Hobert O (2002) *BioTechniques* 32:728–730.
44. Finney M, Ruvkun G (1990) *Cell* 63:895–905.